Designing an enzymatic oscillator: Bistability and feedback controlled oscillations with glucose oxidase in a continuous flow stirred tank reactor

Vladimir K. Vanag,[a] David G. Míguez,[b] and Irving R. Epstein[c]
Department of Chemistry, MS 015, Brandeis University, Waltham, Massachusetts 02454 and Volen Center for Complex Systems, MS 015, Brandeis University, Waltham, Massachusetts 02454

(Received 6 July 2006; accepted 6 October 2006; published online 17 November 2006)

The reaction of glucose with ferricyanide catalyzed by glucose oxidase from *Aspergillus niger* gives rise to a wide range of bistability as the flow rate is varied in a continuous flow stirred tank reactor. Oscillations in *p*H can be obtained by introducing a negative feedback on the autocatalytic production of H^+ that drives the bistability. In our experiments, this feedback consists of an inflow of hydroxide ion at a rate that depends on $[H^+]$ in the reactor as $k_0[OH^-]_0[H^+]/(K+[H^+])$. *p*H oscillations are found over a broad range of enzyme and ferricyanide concentrations, residence times (k_0^{-1}), and feedback parameters. A simple mathematical model quantitatively accounts for the experimentally found oscillations. © *2006 American Institute of Physics*.
[DOI: 10.1063/1.2378833]

I. INTRODUCTION

Oscillatory behavior is ubiquitous in living systems, where it is nearly always associated with enzyme-catalyzed reactions. Examples include glycolytic oscillations in the concentrations of nicotinamide adenine dinucleotide (NADH) and H^+ in pancreatic β-cells, yeast extracts, and reconstituted enzyme systems,[1–6] Ca^{2+} oscillations and waves,[7–9] circadian rhythms,[10,11] and oscillations and waves in neutrophils.[12,13] Since oscillatory preparations extracted from living systems tend to contain a large numbers of species, these systems are often difficult to analyze and poorly characterized. Two exceptions are the peroxidase-oxidase oscillator[14–16] and glycolytic oscillations,[17,18] in which the allosteric enzyme phosphofructokinase (PFK) plays a major role.[19,20] The mechanism of the peroxidase-oxidase oscillator is quite complex.[21] Phosphofructokinase is relatively expensive, and glycolytic oscillation is a multifaceted process that requires several additional enzymes.[22–24]

Many investigators have attempted to find enzymatic *p*H oscillators,[25–31] since the usual bell-shaped dependence of enzyme activity on *p*H implies autocatalysis, a frequently encountered, though neither necessary nor sufficient, element of many chemical oscillators. Early reports of such oscillations with the proteolytic enzyme papain immobilized in a membrane[28,29] did not find confirmation in further investigations.[25,26] The successful introduction of horseradish peroxidase into the hydrogen peroxide–sulfite–ferrocyanide reaction[31] does not represent a true enzymatic oscillator but rather a modification of the existing chemical *p*H oscillator. The enzyme carbonic anhydrase was added to the H_2O_2–Na_2SO_3–Na_2CO_3–H_2SO_4 *p*H oscillator to enhance the negative feedback,[32] essentially in the same manner as horseradish peroxidase was added to the H_2O_2–Na_2SO_3–$Fe(CN)_6^{4-}$ system.[31] We also note the work of Hauser *et al.*[33,34] on oscillations in the hemin-H_2O_2–SO_3^{2-} system, in which hemin, the active center in several enzymes, provides a negative feedback. Although very low *p*H amplitude oscillations occur in glycolysis, these are not driven by $[H^+]$, and the glycolytic oscillator is not therefore a *p*H oscillator.

The goal of designing a simple, inexpensive, enzymatic *p*H oscillator remains attractive, since the discovery of such an oscillator would give strong impetus not only for deeper understanding of enzymatic oscillations but also for studies of pattern formation, owing to the ability of enzymes to be immobilized in thin layers of gel, on various surfaces, or in small compartments.

In this work we present the first experimental and theoretical data on bistability and *p*H oscillations found in the glucose oxidase–glucose–ferricyanide system in a continuous flow stirred tank reactor (CSTR). Because it uses glucose as a fuel, this system is of particular interest, since glucose is a key substrate or nutrient for many organisms. In Sec. II we briefly summarize the properties and the mechanism of catalysis of glucose oxidase (GO). Our strategy for finding oscillations is described in Sec. III. Sec. IV outlines our experimental setup and materials. In Sec. V, we present our results on bistability. In Sec. VI, we experimentally demonstrate how bistability can be converted into oscillations by adding an appropriate feedback. Sections VII and VIII are theoretical, in which we present a model and simulations of oscillations induced by the addition of a negative feedback. Our discussions and conclusions appear in Sec. IX.

II. GLUCOSE OXIDASE

Glucose oxidase (EC 1.1.3.4, from the mold *Aspergillus niger*),[35–37] a flavin-containing [specifically flavin adenine dinucleotide (FAD)] glycoprotein with two subunits of molecular weight ca. 80 kDa each, catalyzes the oxidation of

[a]Author to whom correspondence should be addressed. Electronic mail: vanag@brandeis.edu
[b]Electronic mail: david_miguez@hms.harvard.edu
[c]Electronic mail: epstein@brandeis.edu

β-D-glucose (G) (the first substrate) to glucono-δ-lactone (P) in the presence of a variety of oxidizing (second) substrates, including molecular oxygen (O_2) and many one- and two-electron acceptors. The "ping-pong" mechanism of GO catalysis with O_2 as a second substrate can be expressed as[38]

$$E_{ox} + G \rightarrow E_r + P, \tag{1}$$

$$E_r + O_2 \rightarrow E_{ox} + H_2O_2, \tag{2}$$

where E_{ox} (E_r) is GO in which FAD is in the oxidized (reduced, $FADH_2$) form. Glucono-δ-lactone spontaneously and slowly hydrolyzes to gluconic acid (GA), producing a proton,[38]

$$P + H_2O \rightarrow GA \leftrightarrow (D-\text{gluconate})^- + H^+. \tag{3}$$

If the second substrate of GO is a one-electron acceptor, like ferricyanide (F_i) in our experiments, reaction (2) is replaced by reactions (4) and (5), in which two protons are produced directly in the enzymatic reaction:

$$E_r + F_i \rightarrow E_s + F_e + H^+, \tag{4}$$

$$E_s + F_i \rightarrow E_{ox} + F_e + H^+, \tag{5}$$

where F_e is ferrocyanide and E_s is GO in which FAD is in the semiquinone form, FADH.

Many enzymatic reactions proceed via an intermediate enzyme-substrate complex with Michaelis-Menten kinetics characterized by a Michaelis constant (K_M). A minimal mechanism for GO catalysis, involving two bimolecular steps and one monomolecular step (characterized by the reaction rate constant k_{cat}), gives the following expression for the total enzymatic rate v_e.[36,39]

$$v_e = e_t k_{cat}[S]/([S] + k_{cat}/k_{ox} + k_{cat}[S]/(k_{red}[G])), \tag{6}$$

where e_t is the total concentration of GO, including reduced, semiquinone, and oxidized forms; S is the second substrate (O_2 or F_i, for example); $k_{cat}/k_{ox} = K_{MO}$, the Michaelis constant for the second substrate; $k_{cat}/k_{red} = K_{MG}$, the Michaelis constant for glucose; k_{red} is associated with reaction (1) and k_{ox} with reaction (2) for $S \equiv O_2$ or with reaction (4) or (5) for $S \equiv F_i$.

Usually we use a high concentration of glucose ($[G] \geqslant K_{MG}$), so Eq. (6) can be reduced to the more common Michaelis-Menten expression of the form

$$v_e = e_t k_{cat}[S]/(m[S] + K_{MO}), \tag{7}$$

where $m=1$ for $[G] \gg K_{MG}$ and $m=2$ for $[G] \cong K_{MG}$. Reactions (1)–(5) are all pH dependent. A unique feature of ferricyanide as the second substrate is that the rates of reactions (4) and (5) (i.e., k_{ox}) increase with $[H^+]$,[37,39] thus leading to autocatalysis. From data presented in Ref. 39 we conclude that for typical $[F_i]$ ($\ll$50 mM, when $2[F_i] \ll K_{MO}$, but the relation $[F_i] \gg e_t$ still holds), Eq. (7) can be replaced by the simple expression

$$v_e = k_{ox}[F_i]e_t. \tag{8}$$

Here k_{ox} is proportional to $[H^+]^2$ at pH=2.7–3.3 and $k_{ox} \propto [H^+]$ at pH=3.5–4.0. If we define k'_{ox} by $k_{ox} = k'_{ox}[H^+]$ for pH=3.5–4.0 and k''_{ox} by $k_{ox} = k''_{ox}[H^+]^2$ for pH=2.7–3.3, then[39] $k'_{ox} \cong (1.8 \times 10^7)$ M^{-2} s^{-1} and $k''_{ox} \cong (4 \times 10^{10})$ M^{-3} s^{-1}. At higher pH (4–7), we did not find reliable data and made our own investigation (see Sec. V). Production of $[H^+]$ in this pH range due to reaction (3) is rather slow, about $k_3[P]$, where $k_3 \cong 2.5 \times 10^{-4}$ s^{-1} at pH=6.5 ($k_3 \cong 5 \times 10^{-5}$ s^{-1} at pH=3.5–4.5).[38] Commercial samples of GO may have traces of the enzyme gluconolactonase (EC 3.1.1.17),[40] which catalyzes reaction (3), thus accelerating it.

III. STRATEGY

It is well known that an autocatalytic reaction in a CSTR can give rise to bistability[41] and a bistable system can be transformed into an oscillatory one with an appropriate negative feedback.[42] For example, a large group of inorganic pH oscillators[43,44] involves the autocatalytic production of H^+ (positive feedback) and H^+ consumption (negative feedback). We will use the same strategy for obtaining oscillations in our enzymatic system. To illustrate this approach mathematically, we employ in this section a simplified expression for autocatalytic production of H^+, v_e (the rate of the reaction of oxidation of glucose by ferricyanide catalyzed by GO). To obtain bistability we add to the rate v_e influxes of OH^- and ferricyanide:

$$dh/dt = 2v_e - k_0 h - h_f h[OH^-] + k_b[H_2O], \tag{9}$$

$$d[OH^-]/dt = -k_0[OH^-] + k_0[OH^-]_0 - k_f h[OH^-] + k_b[H_2O], \tag{10}$$

$$ds/dt = -2v_e - k_0(s - s_0), \tag{11}$$

where $s = [F_i]$, $h = [H^+]$, and $v_e = k_a e_t s h$ (k_a is analogous to k'_{ox} introduced above, but we write k_a here, since the real k'_{ox} is a complex expression). The flow terms, which are proportional to k_0, the reciprocal of the residence time, describe not only the constant influx of OH^- and F_i into the CSTR from reservoirs with concentrations $[OH^-]_0$ and s_0, respectively, but the outflow of all mobile species as well. The terms $k_f[H_2O]$ and $k_b h[OH^-]$ describe the water equilibrium:

$$H_2O \leftrightarrow H^+ + OH^-, \quad k_f, k_b. \tag{12}$$

The enzyme is assumed to be immobilized in the reactor, so its total concentration e_t remains constant.

If we set the right hand sides of Eqs. (9)–(11) equal to zero, we obtain a set of algebraic equations that can be solved for the steady state concentrations h_{SS}, $[OH^-]_{SS}$, and s_{SS}. We find $[OH^-]$ and s in terms of h and substitute to obtain a cubic equation for h_{SS} of the form

$$ah^3 + bh^2 + ch + d = 0, \tag{13}$$

with $a = 2k_a e_t$, $b = 2k_a e_t([OH^-]_0 - s_0) + k_0(1 + 2k_a e_t/k_b)$, $c = k_0[OH^-]_0 - 2k_a e_t K_w + (k_0/k_b)(k_0 - 2k_a e_t s_0)$, and $d = -k_0 K_w$ ($K_w = 10^{-14}$ M^2). This equation has three real positive roots, which implies bistability, when $b<0$, $c>0$, and $3[(bc/a - 3d)^2 - 2b^3/9a^2]^2 < 4(c - b^2/3a)^3$. Alternatively, if the water equilibrium, Eq. (12), is established rapidly relative to the other processes, we have $[OH^-] = K_w/h$, so that $d[OH^-]/dt = (-K_w/h^2)dh/dt$, and then

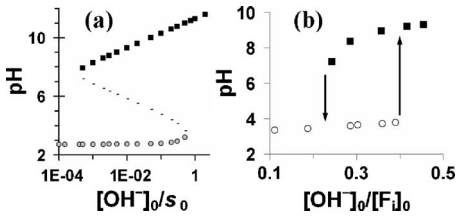

FIG. 1. (a) Bistability in system (15) and (16) at $e_t=10^{-6}$ M, $k_0=2\times10^{-3}$ s^{-1}, $k_a=(7\times10^6)$ M^{-2} s^{-1}, and $s_0=(2\times10^{-3})$ M. Dashes denote unstable steady state. (b) Bistability in a CSTR with influxes of GO, glucose, OH^-, and ferricyanide (F_i). The volume of the reactor, V, is 1.05 ml, $k_0=0.002\,19$ s^{-1}, $[GO]_0=0.33$ mg/ml, $[glucose]_0=21$ mM, $[F_i]_0$ is varied from 2 to 4 mM, and $[OH^-]_0$ is varied from 0.3 to 1 mM, where the subscript 0 denotes input concentrations in the CSTR without reaction.

$$dh/dt - d[\mathrm{OH}^-]/dt = (1 + K_w/h^2)dh/dt, \tag{14}$$

allowing us to rewrite Eqs. (9)–(11) in the simpler form:

$$dh/dt = (1 + K_w/h^2)^{-1}[2v_e - k_0(h + [\mathrm{OH}^-]_0 - K_w/h)], \tag{15}$$

$$ds/dt = -2v_e - k_0(s - s_0). \tag{16}$$

Setting $dh/dt=ds/dt=0$ also gives a cubic equation for h_{SS} of the same form as Eq. (13). The coefficients are identical with the exceptions that the term $k_0(1+2k_ae_t/k_b)$ vanishes from b, and the term $(k_0/k_b)(k_0-2k_ae_ts_0)$ no longer appears in c. Using realistic values for the parameters shows that the dropped terms are quite small under our experimental conditions, and the ranges of bistability obtained by varying, for example, k_0 or the ratio $[OH^-]_0/s_0$, are almost identical whether we use Eqs. (9)–(11) or (15) and (16). An example of such bistability for an experimentally reasonable set of parameters is shown in Fig. 1(a). In Sec. VII, we show that a more detailed analysis gives rise to a two-variable model similar in form to Eqs. (15) and (16).

If we replace the constant influx of OH^- with an appropriate pH-dependent feedback, for example, by substituting $[OH^-]_0h/(K+h)$ for the term $[OH^-]_0$ in Eq. (15), oscillatory behavior can arise.[43] In addition, if, as in our case, the oscillations occur at $p\mathrm{H}<7$, we can simplify Eqs. (15) and (16) by neglecting the terms K_w/h and K_w/h^2:

$$dh/dt = 2v_e - k_0(h + [\mathrm{OH}^-]_0h/(K + h)), \tag{17}$$

$$ds/dt = -2v_e - k_0(s - s_0). \tag{18}$$

A negative feedback of the simple form, $k_0[OH^-]_0h/(K+h)$, used in Eq. (17) is attractive, since it can be realized experimentally by introducing a second enzyme with the usual bell-shaped dependence of activity on pH and an appropriate pK, or alternatively by replacing the flow of OH^- with that of a base A^- with a properly chosen pK_a for the acid-base equilibrium $AH\leftrightarrow A^-+H^+$. In the case of a second enzyme, only the low pH side of the bell-shaped enzyme activity versus pH curve is relevant, yielding a contribution to Eq. (17) proportional to $h/(K+h)$, where the constant term $[OH^-]_0$ is replaced by the maximum velocity of the enzymatic reaction. To ascertain the range of pK at which oscillations can be obtained for GO, we used an artificial feedback, modulating the influx of $[OH^-]_0$ as a function of the pH in the CSTR through a computer.

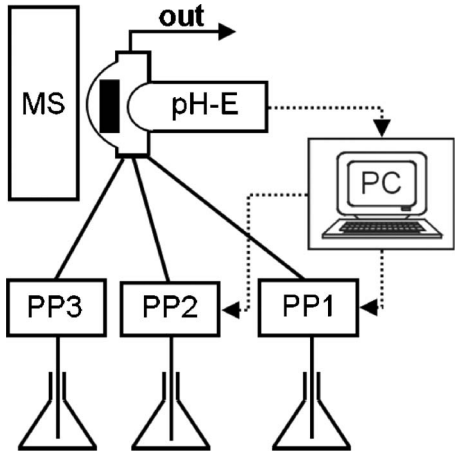

FIG. 2. Experimental setup. pH-E, pH electrode; MS, magnetic stirrer; black bar inside the CSTR is a magnetic stirrer bar; PP1, PP2, and PP3 are peristaltic pumps. Dotted lines are electrical connections. A pH meter between pH-E and PC is not shown. In preliminary experiments we used five pumps (two additional syringe pumps) to vary input concentrations of some reactants.

IV. MATERIALS AND METHODS

The reagents used were glucose oxidase from *Aspergillus niger* (Fluka), potassium ferricyanide [$K_3Fe(CN)_6$, Fluka], sodium hydroxide (NaOH, Fisher), D(+)-glucose anhydrous (Fluka), and catalase (Sigma) (see Appendix A). Stock solutions of ferricyanide and glucose were prepared at least one day before use and kept in the dark (ferricyanide) or the refrigerator (glucose). Glucose was allowed to mutarotate for one day before use.[37]

For CSTR experiments our reactor consisted of a flow pH cell (Cole-Parmer), into which a pH electrode (Cole-Parmer) was inserted (see Fig. 2). The volume V_0 of the reactor was determined by the depth of insertion of the electrode (pH-E in Fig. 2) into the CSTR and varied from 0.16 to 1.1 mL (see Appendix B). The pH electrode was connected to a pH meter (Oakton, Ion 510 series) and further to a computer for data acquisition, feedback generation, and analysis.

In all CSTR experiments we used four primary solutions: (1) NaOH, (2) ferricyanide, (3) GO, and (4) glucose. In the bistability experiments, each solution was fed in through a separate tube. In experiments with negative feedback, the first solution was a mixture of $Fe(CN)_6^{3-}$ and NaOH with $[Fe(CN)_6^{3-}]$ equal to that in the second solution. These two solutions were pumped into the CSTR using computer-controlled peristaltic pumps (PP1 and PP2 in Fig. 2). When the feedback was applied, the residence time in the CSTR (k_0^{-1}) and $[Fe(CN)_6^{3-}]_0$ were kept constant by reducing the speed (R_1) of one of the peristaltic pumps by the same amount as the other (R_2) increased. The velocities of the pumps, R_1 and R_2, were controlled in such a way that the rate of inflow of OH^- was proportional to $h/(K+h)$: $dh/dt=-d[OH^-]/dt=-k_0[OH^-]_0R_1/(R_1+R_2+R_3)=-[OH^-]_0R_1/V_0$ and $R_1=-R_{max}10^{-p\mathrm{H}}/(10^{-p\mathrm{H}}+K)=-R_{max}h/(K+h)$, where R_1

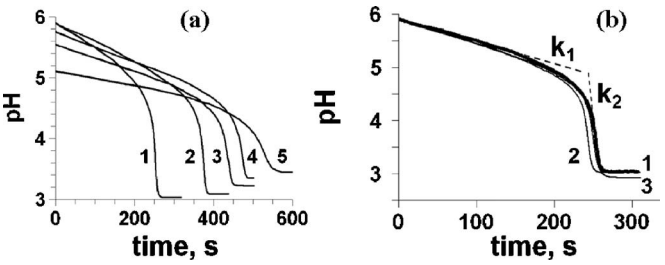

FIG. 3. Reaction of glucose with $Fe(CN)_6^{3-}$ catalyzed by GO in a batch reactor. (a) experiment with $[G]_0=50$ mM, $[O_2]_0=2.7\times10^{-4}$ M, $[Fe(CN)_6^{3-}]_0$/mM=(curve 1) 10, (curve 2) 7.5, (curves 3 and 4) 5, (curve 5) 2.5, and [GO] (mg/ml)=(curves 1–3 and 5) 0.5 and (curve 4) 1. (b) Comparison between experiment (curve 1) and model (C1)–(C3), (C5)–(C11), (C17), and (C18) (curves 2 and 3). For curve 1: (GO)=0.5 mg/ml, $[G]_0=50$ mM, $[Fe(CN)_6^{3-}]_0=10$ mM, and $[O_2]_0=(2.7\times10^{-4})$ M. For curves 2 and 3: $e_t=(6\times10^{-6})$ M (curve 2) and (3×10^{-6}) M (curve 3), $k_1=(3.5\times10^6)$ M^{-2} s^{-1}, $k_2=(3\times10^7)$ M^{-2} s^{-1}, $pK_e=4.0$ ($K=10^{-pK}$ M), $pK_F=3.6$, $[PGO]_0=200e_t$, $pK_G=4.6$, $k_b=10^{10}$ M^{-1} s^{-1}, $k_{fg}=K_Gk_b$, $k_{ff}=K_Fk_b$, $[O_2]_0=2.7\times10^{-4}$ M, $pH_0=5.88$, $s_0=10$ mM, and $k_0=0$.

$+R_2+R_3=V_0k_0$, $R_1+R_2=$constant, R_{max} is the maximum rate of the peristaltic pump, pH is the pH in the CSTR, and we may set our feedback parameter K to any desired value. A peristaltic pump (Rainin Rabbit Plus) was used to pump the third and fourth solutions at a constant rate R_3 in all experiments (PP3 in Fig. 2). These solutions were premixed before entering the cell. Catalase was added to the solution of GO. The solutions were not deoxygenated, so oxygen was supplied to the CSTR together with the other reactants (see below for further discussion of O_2).

For batch experiments we used a large-volume reactor ($V_0=25$ mL) with quartz optical windows. A pH electrode was inserted into the stopper of the reactor. This reactor allowed us to measure simultaneously the pH and the optical density at a chosen wavelength using a homemade spectrophotometric setup.[45]

V. EXPERIMENTAL RESULTS. AUTOCATALYSIS AND BISTABILITY

A typical kinetic run for the reaction of glucose with ferricyanide and oxygen catalyzed by GO under batch conditions is shown in Fig. 3. Reaction with oxygen is very fast, and therefore oxygen is consumed completely in a few seconds, producing H_2O_2 and gluconolactone, both of whose concentrations quickly rise to the initial concentration of oxygen $\cong(2.7\times10^{-4})$ M (table data, see, for example, Ref. 46). Our batch reactor is closed and has no free surface above the solution, so no oxygen can diffuse into the reactor from the atmosphere.

The kinetic curves, measured either with a pH electrode [Fig. 3(a)] or by the absorbance of ferricyanide (not shown), have two distinct regions: a slow region 1 for pH between 6 and 5, and a fast region 2 for pH<4. In Fig. 3(b), the two dashed lines marked as "k_1" and "k_2" denote these regions. In both regions, the reaction is autocatalytic, since the rate (dh/dt) increases with h,[47] as seen by the nearly linear decrease of pH with time.

The autocatalysis in Fig. 3 ceases due to the depletion of ferricyanide as evidenced both optically, by the absorbance measurements, and by the resumption of the reaction on addition of a new portion of ferricyanide. The stoichiometry of reactions (4) and (5) implies that the final h should be equal to $[Fe(CN)_6^{3-}]_0$, which for $[F_i]_0=10$ mM [as in Fig. 3(b)] gives pH=2. We see, however, that the final pH is slightly above 3. Obviously, protons are consumed by $Fe(CN)_6^{4-}$ and/or by some of the amino acid residues of GO. We cannot therefore obtain the rate constants of the autocatalytic reactions simply by measuring the slopes [dashed lines in Fig. 3(b)] of the pH curves. More accurate measurement of the rate constants can be made by examining the time dependence of the $Fe(CN)_6^{3-}$ absorbance. We found that reliable results can also be obtained by fitting a set of experimental pH versus time curves [like those shown in Fig. 3(a)] to theoretical curves deduced from a proposed mechanism for the reaction [see curves 2 and 3 in Fig. 3(b) and Eqs. (C1)–(C3), (C5)–(C11), (C17), and (C18) in Appendix C]. Given (from the literature or additional experiments) the equilibrium constants K_{F1} and K_{F2} for ferrocyanide protonation and K_G for GO protonation, one can deduce the kinetic constants k_1 and k_2 responsible for the first and second stages of autocatalysis.

We observe that a change in enzyme concentration [compare curves 3 and 4 in Fig. 3(a)] leads to only a very slight change in the slope of the kinetic curves, which might suggest that the first slow stage of autocatalysis is independent of the enzyme. For example, this stage might result from hydrolysis of gluconolactone [reaction (3)]. We carried out a set of experiments in which gluconolactone was generated by the reaction of glucose with oxygen in an open reactor catalyzed by GO immobilized in a gel. We found that on removing the gel containing the immobilized GO the rate of H^+ production fell by as much as two orders of magnitude. This result suggests that reaction (3) in the absence of enzyme is not a significant contributor to the slow stage of autocatalysis and that the rate of this stage does depend upon the enzyme concentration. The very weak dependence observed for the rate of this stage on [GO] is explained instead by protonation of GO. If we increase [GO], the rate of production of protons, dh/dt, does increase, but a larger fraction of the protons released in the reaction is consumed by the larger quantity of GO. The protonation of GO balances the increase in dh/dt nearly exactly. The theoretical curves 2 and 3 in Fig. 3(b) illustrate this unusual behavior (see also explanations in Sec. VII).

Glucose oxidase is a large protein with many amino acid residues that can be protonated over a range of pH. Treating these protonation equilibria individually is well beyond our capabilities, and we instead make a major simplification by treating the protonation of GO as if it were a single reaction with a single equilibrium constant K_G:

$$PGOH \leftrightarrow PGO + H^+, \quad K_G. \tag{19}$$

Here, PGO represents a "typical protonatable residue" of GO. If e_t is the total molar concentration of GO and N_{AG} is the average number of protonatable residues (in the pH range between 6 and 3), then

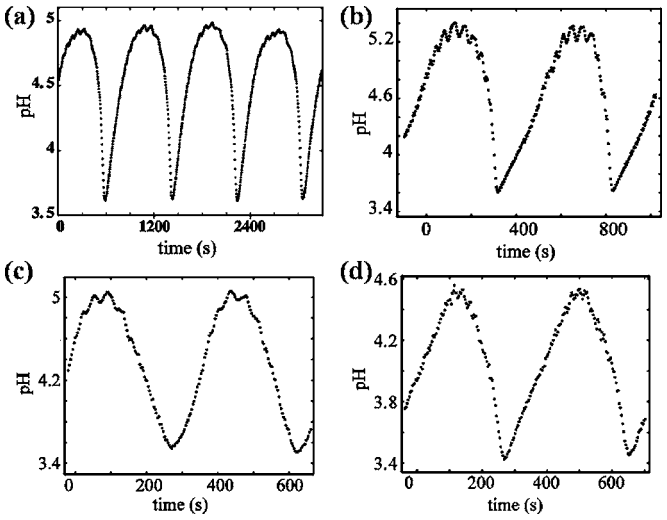

FIG. 4. Experimentally observed pH oscillations in a CSTR for GO-catalyzed oxidation of glucose by ferricyanide supplemented by a negative feedback, $k_0[OH^-]_0 h/(K+h)$. $[catalase]_0=0.01$ mg/ml, $[glucose]_0=50$ mM, and $[GO]_0=1.6$ mg/ml. (a) $[Fe(CN)_6^{3-}]_0=15$ mM, $[NaOH]_0=17$ mM, $k_0=0.003\,29\ s^{-1}$, and $pK=3.9$. (b) $[Fe(CN)_6^{3-}]_0=17$ mM, $[NaOH]_0=15$ mM, $k_0=0.001\,61\ s^{-1}$, and $pK=4.5$. [(c) and (d)] $[Fe(CN)_6^{3-}]_0=17$ mM, $[NaOH]_0=15$ mM, $k_0=0.0091\ s^{-1}$, and $pK=$(c) 4.0 and (d) 3.8.

$$[PGO]_t \equiv [PGO] + [PGOH] = N_{AG} e_t. \tag{20}$$

To estimate pK_G and N_{AG}, we added small amounts of GO to slightly acidic water and measured the pH as a function of $[GO]=e_t$. Fitting the results to the dependence expected from Eq. (19) yields $pK_G \cong 4.6-4.8$ and $N_{AG}=250-200$. These values of pK_G and N_{AG} are used in Eqs. (C1), (C8), and (C9) (see Appendix C) to find values of k_1 and k_2 by fitting these experimental curves to the theoretical ones (see Fig. 3)

In the CSTR with inputs of GO, glucose, $Fe(CN)_6^{3-}$, and NaOH, we easily obtained bistability for many sets of the parameters k_0, $[NaOH]_0/[Fe(CN)_6^{3-}]_0$, and [GO]. An example is shown in Fig. 1(b). The range of parameters at which bistability exists depends, of course, on the parameters, but in all cases we examined this range was narrower than that obtained from the simple theoretical equations (15) and (16), which do not take into account either the protonation of enzyme and product or the two-step autocatalysis with constants k_1 and k_2.

VI. EXPERIMENTAL RESULTS: FROM BISTABILITY TO OSCILLATIONS

Following our strategy, generating oscillations requires that we add a negative feedback to our bistable system. This can be done in a number of ways.[31–33,41] We choose here a "physical" approach, i.e., modulation of the inflow rate of NaOH through a computer. This choice enables us to vary the parameters of the feedback over a very broad range in order to establish the characteristics needed in appropriate chemical feedback agents to be identified in further investigations.

Typical examples of oscillations found in our experiments with the physical feedback $k_0[OH^-]_0 h/(K+h)$ are presented in Fig. 4. The amplitude of the oscillations is generally between pH 3.5 and pH 5. The period ranges from 2 to 20 min, depending on the parameters, especially k_0. The wave form varies as the parameters are changed, but the system usually spends less time at low pH than at high pH.

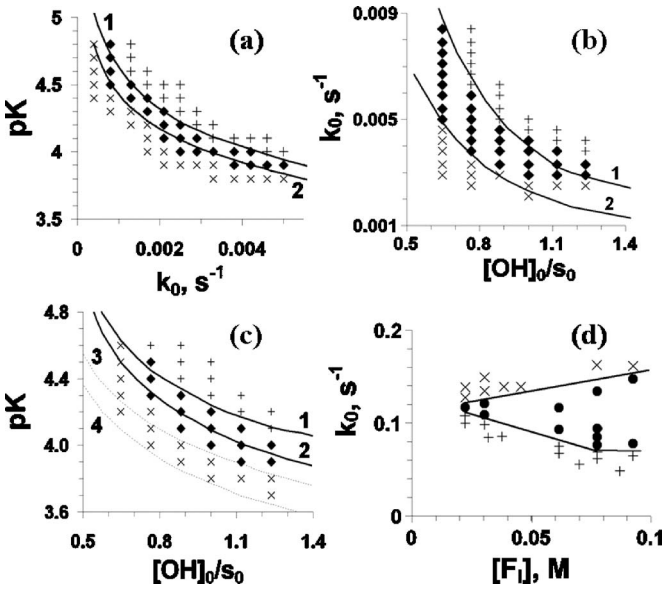

FIG. 5. Experimental and theoretical dynamic phase diagrams. (a) k_0-pK. Experiment (symbols) in a CSTR. Black rhombs denote oscillations, "+" are high pH steady state, and "×" are low pH steady state. Concentrations: $[GO]_0=1.5$ mg/ml, $[catalase]_0=0.01$ mg/ml, $[glucose]_0=50$ mM, $[ferricyanide]_0=17$ mM, and $[NaOH]_0=17$ mM. Curves 1 and 2 are result of linear stability analysis of Eqs. (32) and (33) with parameters $e_t=(9\times10^{-6})$ M, $[PGO]_t=(1.8\times10^{-3})$ M, $k_1=(2.5\times10^6)\ M^{-2}\ s^{-1}$, $k_2=(2.5\times10^7)\ M^{-2}\ s^{-1}$, $pK_e=4$, $s_0=17$ mM, $[OH^-]_0=17$ mM, $pK_F=4.1$, $pK_G=4.6$, and $V_t=0$. Theoretical oscillatory region is between curves 1 and 2; curve 2 is supercritical Hopf bifurcation and curve 1 is subcritical Hopf or saddle bifurcation. (b) $[OH^-]_0/s_0$-k_0. Symbols and parameters as in (a), except $pK=4.0$, $e_t=(8\times10^{-6})$ M, and $[PGO]_t=N_{AG}e_t=(1.6\times10^{-3})$ M. (c) $[OH^-]_0/s_0$-pK. Symbols and parameters as in (a), except $k_0=0.0025\ s^{-1}$ (experiment); $k_0\ (s^{-1})=$(curves 1 and 2) 0.0025 and (curves 3 and 4) 0.006 (calculations); curves 2 and 4 show supercritical Hopf bifurcation; curves 1 and 3 show subcritical Hopf or saddle. Oscillatory region lies between curves 1 (3) and 2 (4). (d) Bistability region for experimental system GO-glucose-ferricyanide in a CSTR, Symbols: full circles, bistability between pH 3 and pH 6; +, low pH; ×, high pH. $[GO]=0.08$ mg/ml and $[glucose]=40$ mM.

In the region of high pH (around pH 5), low amplitude oscillations are observed. These oscillations are artifacts arising from the inevitable pulsations of the peristaltic pump (PP). The frequency of these small-amplitude oscillations is completely determined by the PP rotation frequency. If we increase the volume of the CSTR, these oscillations decrease in amplitude.

Several diagrams showing the parameter regions in which oscillations occur are presented in Figs. 5(a)–5(c). The ranges of pK, k_0, and $[OH^-]_0/[F_i]_0$ are quite broad: pK can vary at least between 3.8 and 4.6 and $[OH^-]_0/[F_i]_0$ can lie between 0.7 and 1.3. Note that we have established the upper and lower boundaries of the oscillatory domain while the left and right boundaries remain unknown. The large expenditure of enzyme in the CSTR experiments prevented us from delineating the entire domain of oscillation. Even though the enzyme is relatively cheap, determining each point in our diagrams required on average at least 20 mg of enzyme, so that 2 g of the enzyme were consumed for each frame in Fig. 5.

VII. MODELING

Equations (15), (16) or (17), (18) provide a simple two-variable model that can be analyzed analytically without integration of the rate equations, for example, by using linear stability analysis. They do, however, neglect many details of the kinetics of the system. Our goal here is to develop a similar set of general equations for an enzymatic *p*H oscillator starting from a full set of chemical reactions:

$$E_{ox} + G \rightarrow E_r + P, \quad k_g = k_{red}[G], \tag{21}$$

$$O_2 + E_r \rightarrow H_2O_2 + E_{ox}, \quad k_{ox}, \tag{22}$$

$$P + H_2O \rightarrow B + H^+, \quad v_3, \tag{23}$$

$$2S + E_r \rightarrow 2F_e + E_{ox} + 2H^+, \quad v_S, \tag{24}$$

$$PGOH \leftrightarrow PGO + H^+, \quad K_G, \tag{25}$$

$$F_eH \leftrightarrow F_e + H^+, \quad K_{F1}, \tag{26}$$

$$F_eH_2 \leftrightarrow F_eH + H^+, \quad K_{F2}, \tag{27}$$

$$SH \leftrightarrow S + H^+, \quad K_S, \tag{28}$$

$$VH \leftrightarrow V + H^+, \quad K_V. \tag{29}$$

Here, the substrate S is $Fe(CN)_6^{3-}$, F_e is $Fe(CN)_6^{4-}$, P is D-glucono-δ-lactone, G is β-*D*-glucose, B is unprotonated D-gluconic acid, PGO represents a protonatable GO residue as discussed in Sec. V, F_eH, F_eH_2, and SH are protonated forms of F_e and S; and V and VH, introduced for the sake of generality, are unprotonated and protonated forms of an arbitrary species that can be introduced into the reactor. For example, V could be an additional base or a new species such as a *p*H indicator or buffer.

Reactions (21)–(24), which are identical to reactions (1)–(4), respectively, have been discussed above. We take $[G]$=constant$\gg[S]$ ($\equiv s$); we write $k_g = k_{red}[G]$ or $k_g = k_{cat}$ [see Eq. (6)]. For reactions (23) and (24), we use the actual *p*H-dependent rate expressions for v_3 and v_S. Fitting experimental curves such as curve 1 in Fig. 3(b) with simulated curves derived from various expressions for v_s, we found that the best result is obtained with

$$v_S = [E_r]sh(k_1K_e^n + k_2h^n)/(K_e^n + h^n), \quad n = 2. \tag{30}$$

Equation (30) gives $v_S \cong k_1[E_r]sh$ when $h \ll K_e$ and $v_S \cong k_2[E_r]sh$ when $h \gg K_e$. The fits imply that $k_2 \gg k_1$ and $pK_e \cong 4$. Analysis of data for gluconolactone hydrolysis[38] implies that v_3 can be expressed as

$$v_3 = [P][k_{33}/(h + K_{gl}) + k_3], \tag{31}$$

with $k_3 \cong 5 \times 10^{-5}$ s^{-1}, $k_{33} \cong (3 \times 10^{-11})$ M^{-1} s^{-1}, and $K_{gl} \cong (3 \times 10^{-8})$ M. We show in Appendix C that the rather slow rate v_3 can be neglected.

The protonation constant K_G was estimated in Sec. V. Several values for K_{F1} can be found in the literature: $10^{-3.2}$ M,[48] $10^{-3.7}$ M,[49] and $10^{-4.1}$ M.[50] In the fundamental work on the protonation of hexacyanoferrates,[51] it was found that pK_{F1}=4.2 [$K_F = (6.7 \times 10^{-5})$ M] for zero ionic strength (IS) (actually, at IS$<$0.01) and pK_{F1}=3.2 at IS=0.1. The second protonation [Eq. (27)], with pK_{F2}=2.22 [$K_{F2} = (6 \times 10^{-3})$ M] at IS=0 may be important at small IS and low *p*H. Protonation of ferricyanide with equilibrium constant pK_S will be neglected here, since $pK_S < 1$,[51,52] though addition of ferricyanide to pure (or slightly acidic) water increases the *p*H significantly at large $[S]$ ($>$10 mM), and thus this process should be taken into account in more detailed models.

In Appendix C, we show that by using the information above the rate equations for our full scheme, Eqs. (21)–(29) at *p*H$<$7 can be reduced to the two-variable model of Eqs. (32) and (33),

$$dh/dt = [2v_S - k_0h - k_0[OH^-]_0h/(K + h) - k_0(s_0 - s)h/(K_{F1} + h) - k_0V_th/(K_V + h)]/D, \tag{32}$$

$$ds/dt = -2v_S - k_0(s - s_0), \tag{33}$$

where

$$v_S = e_tsh(k_1K_e^2 + k_2h^2)/(K_e^2 + h^2) \tag{34}$$

and

$$D = [1 + N_{AG}e_tK_G/(K_G + h)^2 + (s_0 - s)K_{F1}/(K_{F1} + h)^2 + V_tK_V/(K_V + h)^2]. \tag{35}$$

In Appendix D, we summarize all symbols and abbreviations we use in Eqs. (32)–(35).

Comparing Eqs. (32) and (33) to Eqs. (17) and (18), we can assess the role of the protonation reactions (25), (26), and (29) in the *p*H oscillations. Looking at Eq. (32), we note two additional terms in the numerator plus the appearance of the denominator D. The terms $k_0(s_0-s)h/(K_{F1}+h)$ and $k_0V_th/(K_V+h)$ have the same form as the term $k_0[OH]_0h/(K+h)$ and can thus play similar roles in providing feedback. This implies that oscillations or bistability can in general occur even without the artificial feedback term (OH^- influx), if (s_0-s) and K_{F1} or V_t and K_V have appropriate values. We demonstrate this type of bistability experimentally in Sec. IX. In essentially the same manner, with a "bufferlike negative feedback," Hauser *et al.*[33] and Frerichs and Thompson[32] used hemin and bicarbonate, respectively, to obtain *p*H oscillations in the hydrogen peroxide–sulfite autocatalytic system.

The denominator D in Eq. (32) decreases dh/dt and decelerates the autocatalysis. Each protonation-deprotonation equilibrium of a mobile species, e.g., Eqs. (25)–(29), contributes to D a term of the form $[A]_tK_a/(K_a+h)^2$, where K_a is the equilibrium constant for the association reaction $AH \leftrightarrow A^- + H^+$. If $[A]_t > K_a$, then $[A]_tK_a/(K_a+h)^2$ can be greater than 1 and consequently this equilibrium can decrease dh/dt significantly. If, in a batch experiment (k_0=0), e_t is high enough to make $N_{AG}e_tK_G/(K_G+h)^2$ both the largest term in D and much larger than 1, then both the numerator and the denominator of dh/dt will be proportional to e_t, yielding a rate independent of the total enzyme concentration, in agreement with the result shown in the kinetic curve in Fig. 3(b) and discussed in the fourth paragraph of Sec. V.

The fact that the rate v_S is directly proportional to e_t [Eq. (34)] implies that it should be possible to vary the period of oscillations of this type over a broad range. Suppose we carry out a set of CSTR experiments in which e_t is directly proportional to k_0, $e_t=Ck_0$. If we introduce a dimensionless time $\tau=tk_0$ into Eqs. (32) and (33), the rescaled equations are independent of e_t and k_0 [or nearly so, since e_t still appears in D via Eq. (35)]. The actual period of oscillations is proportional to k_0^{-1} and thus is limited only by the flow rate range of the pump and the concentration of enzyme in the stock solution. Such large variations of the oscillation period are unknown in nonenzymatic pH oscillators. This analysis also implies that the boundaries of the oscillatory region should approach straight lines of the form $e_t=C_1k_0$ and $e_t=C_2k_0$ [see Fig. 7(a)].

VIII. LINEAR STABILITY ANALYSIS AND SIMULATIONS

Much of our investigation of Eqs. (32) and (33) and Eqs. (17) and (18) employed linear stability analysis. We also carried out direct numerical integration of these equations using the FLEXPDE software package.[53] We considered the simplest case of $V_t=0$ (no V species) that corresponds to our experiments with artificial feedback. We refer to Eqs. (32)–(35) with $V_t=0$ as model A. In Figs. 5(a)–5(c), we show the experimentally observed and calculated oscillatory regions in the k_0-pK, $[OH^-]_0/s_0$-k_0, and $[OH^-]_0/s_0$-pK, parameter planes. The agreement between experiment and theory is encouraging.

To illustrate the sensitivity of model A to k_0, we present in Fig. 5(c) theoretical results for two different flow rates. Further analysis reveals that the oscillatory region is quite sensitive to k_2, e_t, and K_{F1} as well. The parameters k_2 (see Appendix E) and K_{F1} are more difficult to estimate than $[OH^-]_0/s_0$, pK, or k_0, since the first two depend on ionic strength and/or ferricyanide concentration in poorly characterized ways, while the latter group can be controlled directly by the experimenter. To calculate the molar concentration of enzyme, e_t, from the measured value in mg/ml, we used a molecular weight for a two-subunit GO of 155 000,[35,37] but this value may not be completely accurate, since we used commercial enzyme without further purification.

In comparing experimental and theoretical data we should also keep in mind the simplifications made in our model, particularly the use of a single pK_G to characterize the protonation of the enzyme [Eq. (25)] and our neglect in the model of the few second delay, arising from the response time of the pH electrode, between changes in the pH in the CSTR and the resulting changes in the feedback (inflow rate of OH^-).

In Fig. 6, we show calculated oscillatory domains for a much broader range of the parameters k_0 and $[OH^-]_0/s_0$. The oscillatory domain in Fig. 6(b) extends to $[OH^-]_0=0$ (no artificial feedback), while in Fig. 6(a) this domain ends at $[OH^-]_0/s_0\cong 0.1$. Though several parameters differ slightly between Figs. 6(a) and 6(b), additional analytical calculations indicate that the main source of this difference is the value of pK_{F1}. For small pK_{F1} [=3.2 in Fig. 6(a)], oscillation is impossible at $[OH^-]_0=0$. For larger pK_{F1} [=4.0 in Fig. 6(b)], oscillation at $[OH^-]_0=0$ can occur as a result of the term $-k_0(s_0-s)h/(K_{F1}+h)$ in Eq. (32), which arises from the equilibrium (26), a so-called bufferlike negative feedback.

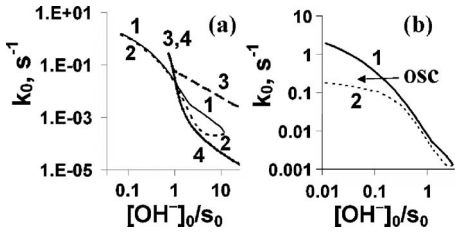

FIG. 6. Linear stability analysis of Eqs. (32) and (33) at $V_t=0$ (curves 1 and 2 in a and b) and eqs. (17) and (18) (a, curves 3 and 4). Oscillatory regions are between curves 1 and 2 for model (32) and (33) and between curves 3 and 4 for for model (17) and (18). Curve 1 is subcritical Hopf line or saddle, curve 2 is supercritical Hopf bifurcation. Parameters for curves 1 and 2 in (a): $e_t=10^{-5}$ M, $[PGO]_t=(2\times10^{-3})$ M, $s_0=17$ mM, $k_1=(3.5\times10^6)$ M^{-2} s^{-1}, $k_2=(3\times10^7)$ M^{-2} s^{-1}, $pK_e=4$, $pK=4$, $pK_{F1}=3.2$, and $pK_G=4.6$. Parameters for curves 3 and 4 in (a) $k_ae_t=300$, $s_0=17$ mM, and $pK=4$. (b) $e_t=(1.5\times10^{-5})$ M, $[PGO]_t=N_{AG}e_t$, $N_{AG}=200$, $s_0=17$ mM, $k_1=(3.0\times10^6)$ M^{-2} s^{-1}, $k_2=(2.5\times10^7)$ M^{-2} s^{-1}, $pK_e=4$, $pK=4.1$, $pK_{F1}=4$, and $pK_G=4.6$.

The broad oscillatory domain in Fig. 6(a) between curves 1 and 2 for $1<[OH^-]_0/s_0<10$ results from the artificial feedback, $k_0[OH^-]_0h/(K+h)$. In the absence of the protonation-deprotonation reactions (25) and (26), we would expect this region to be even larger. To examine this question, we recalculated the oscillatory domain for system (17) and (18) with the same parameters but without the protonation equilibria. We see [curves 3 and 4 in Fig. 6(a)] that the oscillatory domain is indeed much broader. Note that a very narrow oscillatory region exists even when $[OH^-]_0<s_0$, at $0.7<[OH^-]_0/s_0<1$ (where curves 3 and 4 almost merge).

The dependence of the oscillatory region and frequency of oscillation on k_0 and e_t are shown in Fig. 7(a). As we argued at the end of Sec. VII, the oscillatory region should be bounded by straight lines $e_t=C_1k_0$ and $e_t=C_2k_0$. Indeed, curve 2 is very well fitted by this expression with $C_2=0.001\,25$, while only the lower left portion of curve 1 is well described by $e_t=C_1k_0^n$ with $C_1=0.002\,36$ and $n=0.93$. At larger e_t, when the term $N_{AG}e_tK_G/(K_G+h)^2$ in the denominator [Eq. (35)] becomes significant, curves 1 and 2 merge, and the frequency [curve 3 in Fig. 7(a)] tends to be independent of k_0 if (k_0,e_t) lie close to curve 1. Figure 7(b)

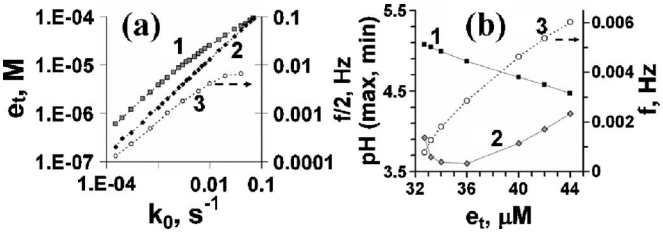

FIG. 7. (a) Diagram k_0-e_t for model (32) and (33). Oscillatory region is between curves 1 and 2. Curve 3 is frequency of oscillations for parametric points that are very close to curve 1. For curve 1, $e_t=0.002\,277(k_0)^{0.9312}$; for curve 2, $e_t=0.001\,258(k_0)^{0.9897}$. (b) Typical dependence of the frequency (curve 3) and amplitude of pH oscillations for model (32) and (33) at constant k_0. Curves 1 and 2 are the maximum and minimum of pH oscillations. Parameters: $k_1=(7\times10^6)$ M^{-2} s^{-1}, $k_2=(6\times10^7)$ M^{-2} s^{-1}, $pK_e=4$, $pK=4$, $[PGO]_t=200e_t$, $pK_G=4.6$, and $v_0=0$; (a) $s_0=17$ mM, $[OH^-]_0=34$ mM, and $pK_{F1}=3$; (b) $k_0=0.016$ s^{-1}, $s_0=12$ mM, $[OH^-]_0=30$ mM, and $pK_{F1}=2.9$.

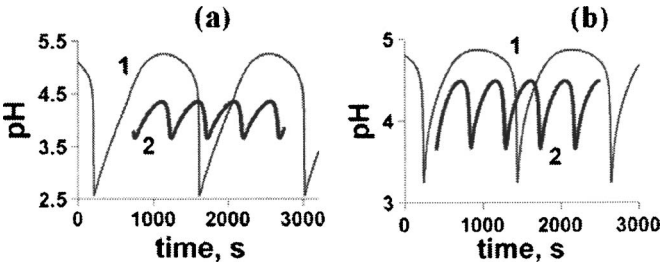

FIG. 8. Examples of oscillations in model (32) and (33) at $V_t=0$. Parameters: $[PGO]_t=200e_t$, $pK_G=4.6$, $pK_e=4$, $k_1=(3.5\times10^6)$ M^{-2} s^{-1}, and $k_2=(3\times10^7)$ M^{-2} s^{-1}; (a) $e_t=12$ μM, $k_0=0.0028$ s^{-1}, $s_0=15$ mM, $[OH^-]_0=26$ mM, $pK=$(curve 1) 4.1 and (curve 2) 4.05 and $pK_{F1}=3.0$; (b) $e_t=20$ μM, k_0 $(s^{-1})=$(curve 1) 0.0087 and (curve 2) 0.0084, $s_0=13$ mM, $[OH^-]_0=20$ mM, $pK=4$, and $pK_{F1}=3.6$.

demonstrates how the frequency and amplitude of oscillations change with e_t at constant k_0. At large e_t [corresponding to curve 1 in Fig. 7(a)], the Hopf bifurcation is supercritical, and the amplitude of oscillations grows slowly as e_t decreases. When e_t approaches the minimum that permits oscillation [corresponding to curve 2 in Fig. 7(a)], the amplitude and period are relatively large and, in most cases, this boundary represents a subcritical Hopf bifurcation.

To conclude our analysis, we present several examples of oscillations (Fig. 8) found by numerical integration of model A. We find a variety of wave forms, including those seen in our experiments. Small changes in parameters [pK in Fig. 8(a) and k_0 in Fig. 8(b)] can give rise to significant changes in oscillatory dynamics.

IX. DISCUSSION AND CONCLUSION

Once the principles of chemical oscillation were sufficiently well understood to allow the construction of the first deliberately designed chemical oscillator,[54] dozens of new oscillators soon followed.[55] Ten years ago Ohmori and Yang[26] wrote that, "There is a strong need for the researches in the areas of biotechnology and nonlinear dynamics to have some simple, robust and easily reproducible immobilized-enzyme systems to serve as model systems for studying the dynamics of nonlinear reaction-diffusion systems." The GO-glucose-ferricyanide system studied in this work can serve as a model system of the sort envisioned by Ohmori and Yang. GO is a stable and cheap enzyme that can be easily immobilized. There are hundreds, if not thousands, of papers about applications for GO with various methods of immobilization.

Our system with an appropriate negative feedback, here a computer-assisted feedback, can be considered as the first designed enzymatic pH oscillator, in which an autocatalytic enzymatic reaction plays the major role. An obvious next step is to replace the computer-assisted feedback by other enzymatic or chemical reactions to serve as the chemical negative feedback. The theory developed in this study should be helpful in identifying these reactions. Our Eqs. (32)–(35) show that any chemically inert species able to capture protons with an appropriate pK_a can provide this negative feedback. However, there is an obvious difference between our computer-controlled feedback [the term $k_0[OH^-]_0h/(K+h)$ in Eq. (32)] and a feedback originating from an actual protonation equilibrium (29), which gives rise to terms $k_0V_th/(K_V+h)$ in the numerator and $V_tK_V/(K_V+h)^2$ in the denominator of Eq. (32) [see Eq. (35)]. The additional term in the denominator can significantly decrease the rate of reaction and prevent the system from oscillationing, even at "good" parameters V_t and K_V that correspond to $[OH^-]_0$ and K, respectively, for which oscillations occur with computer-controlled feedback. Our preliminary efforts with some likely candidates for the chemical feedback species V have not yet borne fruit, probably because of this effect.

In our system, the feedback role can, in principle, even be played by a product of the GO reaction, i.e., by ferrocyanide. In this case, the second protonation (27) and the protonation of ferricyanide (28) should be taken into account. Analysis of model (C36)–(C39) (see Appendix C) reveals that oscillations in general are possible in this still simplified model with only ferricyanide, glucose, and GO, *if* both pK_{F1} and [ferricyanide] are large enough. However, as [ferricyanide] increases, the ionic strength also goes up, causing pK_{F1} to decrease. The dependence of pK_{F1} on ionic strength[51] and our analysis show that pK_{F1} changes with the growth of [ferricyanide] in such a way that oscillations in the actual experimental system will be inaccessible, in agreement with our observations. Nevertheless, the negative feedback from the protonation of ferrocyanide is strong enough to produce bistability.

The bistability region found experimentally at high input concentrations of ferricyanide and no OH^- influx is shown in Fig. 5(d). This bistability region is described only qualitatively, not quantitatively, by Eqs. (C36)–(C39) for two reasons. Expression (C39) for v_S at low $p\mathrm{H}\approx3$ is not correct, since v_S is proportional to h^2 in this pH range[39] as noted in our discussion of Eq. (8), not to h, as in Eq. (C39). We also observed (see Appendix F) an irreversible inhibition of GO by ferricyanide at low pH in the absence of glucose.

Our enzymatic pH oscillator is a typical "depleted substrate-type" oscillator that can function most easily in a CSTR, since the depleted substrate (here ferricyanide) must be replenished. If, however, additional reactions can regenerate ferricyanide from ferrocyanide (for example, with the aid of a peroxidase), then it should be possible to create a batch oscillator.

The concentration of glucose oscillates in our system in the same manner as the concentration of ferricyanide, though the relative amplitude is smaller, since [glucose] $>$[ferricyanide]. If an additional glucose-dependent enzymatic reaction is coupled to the present system, then this reaction can also oscillate. Such coupled reactions can be catalyzed, for example, by hexokinase, glucokinase, glucose dehydrogenase, glucomylase, or gluconase.

Preliminary experiments with GO immobilized in a polyacrylamide gel reveal that this system, in the bistable regime, supports pH front propagation and pulse propagation, making it an excellent candidate for further pattern formation investigation. By coupling a thin layer of this preparation with another layer containing a different immobilized enzyme, such as horseradish peroxidase or urease, one can study the role of delay between two layers with positive and negative feedbacks. There are a number of theoretical works

in which immobilized enzymes are used in membrane oscillators. For example, the ability of GO to produce protons was used to regulate the permeability of a poly(*N*-isopropyl acrylamide-co-methacrylic acid) membrane to give chemomechanical oscillations.[56] With the prospect of simple, cheap, enzymatic oscillators, the outlook for nonlinear biochemical engineering in reaction-diffusion systems is bright indeed.

ACKNOWLEDGMENT

This work was supported by National Science Foundation Grant Nos. CHE-0306262 and CHE-0615507.

APPENDIX A: PRUSSIAN BLUE AND CATALASE

The enzyme catalase catalyzes the disproportionation of H_2O_2 produced in reaction (22), thereby suppressing both the undesirable back reaction $2H^+ + 2F_e + H_2O_2 \rightarrow 2F_i + 2H_2O$ (with rate constant $k_{uw} = 1.6 \times 10^{-4}$ s^{-1}, which is independent of $[H^+]$ and $[F_e]$ in our concentration range[52]) and the very slow formation of a blue precipitate, which is actually Prussian Blue[57] and which is formed in reaction(s) of F_i or F_e with Fe^{2+} or Fe^{3+}, respectively, in the presence of CN^-, generated by the slow destruction of F_e promoted by H_2O_2. The concentration of catalase is determined from the inequality $[\text{catalase}] > n_f(k_0 + k_{uw})/k_c$, where k_c is the rate constant for H_2O_2 disproportionation catalyzed by catalase, and we seek to decrease $[H_2O_2]$ by a factor n_f. With $k_0 = (10^{-3} - 10^{-2})$ s^{-1}, $k_c = 10^7$ M^{-1} s^{-1}, and $n_f = 10$, we need $[\text{catalase}] > 10^{-8}$ M, which is equivalent to 0.0025 mg/ml (for $M_{\text{catalase}} = 240\,000$). We used $[\text{catalase}] = 0.01$ mg/ml.

APPENDIX B: MEASUREMENT OF V_0

The volume V_0 of the CSTR was measured kinetically from the equation $(h - h_f) = (h_0 - h_f)\exp(-tR_f/V_0)$, where R_f is a known flow rate (ml/s), and h_0 and h_f are the initial and final concentrations of $[H^+]$, respectively; h_0 was established by a jump in the inflow rate of a weak acid.

APPENDIX C: DERIVATION OF MODEL (32)–(35)

The rate equations for reactions (21)–(29) at $p\text{H} < 7$ in a CSTR are

$$dh/dt = 2v_S + v_3 - k_0[h + [\text{OH}^-]_0 h/(K + h)] - k_b[F_e]h + k_{ff}[F_e\text{H}] - k_b s h + k_{fs}[S\text{H}] - k_b[F_e\text{H}]h + k_{ff2}[F_e\text{H}_2] - k_b[\text{PGO}]h + k_{fg}[\text{PGOH}] - k_b[V]h + k_{fv}[V\text{H}], \tag{C1}$$

$$ds/dt = -2v_S - k_b s h + k_{fs}[S\text{H}] - k_0(s - s_0), \tag{C2}$$

$$d[S\text{H}]/dt = k_b s h - k_{fs}[S\text{H}] - k_0[S\text{H}], \tag{C3}$$

$$d[P]/dt = k_g[E_{\text{ox}}] - v_3 - k_0[P], \tag{C4}$$

$$d[F_e]/dt = 2v_S - k_b[F_e]h + k_{ff}[F_e\text{H}] - k_0[F_e], \tag{C5}$$

$$d[F_e\text{H}]/dt = k_b[F_e]h - k_{ff}[F_e\text{H}] - k_b[F_e\text{H}]h + k_{ff2}[F_e\text{H}_2] - k_0[F_e\text{H}], \tag{C6}$$

$$d[F_e\text{H}_2]/dt = k_b[F_e\text{H}]h - k_{ff2}[F_e\text{H}_2] - k_0[F_e\text{H}_2], \tag{C7}$$

$$d[\text{PGO}]/dt = -k_0[\text{PGO}]h + k_{fg}[\text{PGOH}] - k_0'([\text{PGO}] - [\text{PGO}]_t), \tag{C8}$$

$$d[\text{PGOH}]/dt = k_b[\text{PGO}]h - k_{fg}[\text{PGOH}] - k_0'[\text{PGOH}], \tag{C9}$$

$$d[V]/dt = -k_b[V]h + k_{fv}[V\text{H}] - k_0([V] - v_t), \tag{C10}$$

$$d[V\text{H}]/dt = k_b[V]h - k_{fv}[V\text{H}] - k_0[V\text{H}], \tag{C11}$$

$$d[E_{\text{ox}}]/dt = -k_g[E_{\text{ox}}] + v_S + k_{\text{ox}}[\text{O}_2][E_r] - k_0'[E_{\text{ox}}], \tag{C12}$$

$$d[E_r]/dt = k_g[E_{\text{ox}}] - v_S - k_{\text{ox}}[\text{O}_2][E_r] - k_0'([E_r] - e_t), \tag{C13}$$

$$d[\text{O}_2]/dt = -k_{\text{ox}}[\text{O}_2][E_r] - k_0([\text{O}_2] - [\text{O}_2]_0), \tag{C14}$$

where $k_b = (10^9 - 10^{10})$ M^{-1} s^{-1} (diffusion controlled bimolecular reaction rate constant for all protonation steps), $k_{ff} = k_b K_{\text{F1}}$, $k_{ff2} = k_b K_{\text{F2}}$, $k_{fg} = k_b K_{\text{G}}$, $k_{fv} = k_b K_V$, $k_{fs} = k_b K_S$, and v_S and v_3 are given by Eqs. (30) and (31), respectively. The term proportional to $[\text{OH}^-]_0$ in Eq. (C1) arises from the form chosen for the inflow of hydroxide ion and the elimination of $[\text{OH}^-]$ as a variable via the same procedure used in Sec. III to arrive at Eq. (17). The terms proportional to k_0' in Eqs. (C8), (C9), (C12), and (C13) reflect the fact that the enzymatic species in general may have a different flow rate from the other species in the system, for example, for enzyme immobilized in the reactor $k_0' = 0$. If the enzyme flows in and out with the other species, which is the case for our experiments in a CSTR, then $k_0' = k_0$.

We first make a quasi-steady-state approximation for the GO species and oxygen, setting $d[E_{\text{ox}}]/dt = d[E_r]/dt = d[\text{O}_2]/dt = 0$ to eliminate Eqs. (C12)–(C14), since reactions (21) and (22) are fast. The conservation of enzyme species implies that $[E_r] + [E_{\text{ox}}] = e_t$ (the semiquinone form E_s is omitted for simplicity). From Eq. (C14) we deduce that

$$[\text{O}_2]_{\text{SS}} = k_0[\text{O}_2]_0/(k_{\text{ox}}[E_r] + k_0) \cong k_0[\text{O}_2]_0/(k_{\text{ox}}[E_r]), \tag{C15}$$

where we have used the fact that $k_{\text{ox}}[E_r] = (1 - 10)$ s$^{-1} \gg k_0 = (10^{-3} - 10^{-2})$ s^{-1}. Under our experimental conditions,

$$k_g \gg k_{\text{ox}}[\text{O}_2]_{\text{SS}} \text{ and } k_g \gg sh(k_1 K_e^n + k_2 h^n)/(K_e^n + h^n),$$

which implies that $[E_r] \gg [E_{\text{ox}}]$ or $[E_r] \cong e_t$.

From Eq. (C13) with the aid of (C15) and inequalities $[\text{O}_2]_0 > e_t \gg [E_{\text{ox}}]$, we have

$$k_g[E_{ox}] \cong v_S + k_{ox}[O_2]_{SS}[E_r] - k_0'[E_{ox}] \cong v_S + k_0[O_2]_0. \tag{C16}$$

Equations (C4) and (30) may now be rewritten as

$$d[P]/dt = v_S + k_0[O_2]_0 - v_3 - k_0[P], \tag{C17}$$

$$v_S = e_t sh(k_1K_e^2 + k_2h^2)/(K_e^2 + h^2). \tag{C18}$$

The simulations shown in Fig. 3(b) were obtained using this modified set of equations (C1)–(C3), (C5)–(C11), (C17), and (C18), under batch conditions ($k_0=0$) and neglecting the equilibria in Eqs. (27)–(29). Fitting these equations to the experimental curves shown in Fig. 3(a) yielded the values of k_1, k_2, K_e (at $n=2$), and pK_{F1} given in the captions to Fig. 3.

We can simplify our set of equations further by eliminating the fast protonation-deprotonation[58,59] reactions. Note first that the pairs of equations (C8)–(C9) and (C10)–(C11) are identical from a mathematical point of view, and summing (C8) and (C9) as well as (C10) and (C11) implies that $[PGO]+[PGOH]=[PGO]_t$ and $[V]+[VH]=V_t$. This allows us to decrease the number of variables and rewrite (C1) and, for example, (C9) as

$$\begin{aligned} dh/dt = {} & 2v_S + v_3 - k_0[h + [OH^-]_0h/(K+h)] - k_b[F_e]h \\ & + k_{ff}[F_eH] - k_bsh + k_{fs}[SH] - k_b[F_e]h \\ & + k_{ff2}[F_eH_2] - k_b[PGO]h + k_{fg}([PGO]_t - [PGO]) \\ & - k_b[V]h + k_{fv}[VH], \end{aligned} \tag{C19}$$

$$\begin{aligned} -d[PGO]/dt &= d[PGOH]/dt \\ &= k_b[PGO]h - k_{fg}([PGO]_t - [PGO]) \\ &\quad - k_0'([PGO]_t - [PGO]). \end{aligned} \tag{C20}$$

Using equilibria (26)–(29) we can write

$$[PGO]h = K_G[PGOH], \tag{C21}$$

$$[F_e]h = K_F[F_eH], \tag{C22}$$

$$[F_eH]h = K_{F2}[F_eH_2], \tag{C23}$$

$$[S]h = K_S[SH], \tag{C24}$$

$$[V]h = K_V[VH]. \tag{C25}$$

Introducing the mass balances $[PGO]+[PGOH]=[PGO]_t$, $[F_e]+[F_eH]+[F_eH_2]=F_t$, $[S]+[SH]=S_t$, and $[V]+[VH]=V_t$ gives

$$[PGOH] = [PGO]_th/(h + K_G), \tag{C26}$$

$$[F_eH] = F_t/(1 + K_{F1}/h + h/K_{F2}), \tag{C27}$$

$$[F_eH_2] = F_t/(1 + K_{F2}/h + K_{F1}K_{F2}/h^2), \tag{C28}$$

$$[SH] = S_th/(h + K_S), \tag{C29}$$

$$[VH] = V_th/(h + K_V), \tag{C30}$$

and then

$$\begin{aligned} & h + [PGOH] + [F_eH] + 2[F_eH_2] + [SH] + [VH] \\ & \quad \equiv h + [PGO]_th/(h + K_G) + F_t/(1 + K_{F1}/h + h/K_{F2}) \\ & \qquad + 2F_t/(1 + K_{F2}/h + K_{F1}K_{F2}/h^2) + S_th/(h + K_S) \\ & \qquad + V_th/(h + K_V). \end{aligned} \tag{C31}$$

Differentiating Eq. (C31) with respect to time gives

$$\begin{aligned} & dh/dt + d[PGOH]/dt + d[F_eH]/dt + 2d[F_eH_2]/dt \\ & \quad + d[SH]/dt + d[VH]/dt = (dh/dt)D, \end{aligned} \tag{C32}$$

where

$$\begin{aligned} D = {} & 1 + [PGO]_tK_G/(K_G + h)^2 + F_tK_{F2}(K_{F1}K_{F2} + 4hK_{F1} \\ & + h^2)/(K_{F1}K_{F2} + hK_{F2} + h^2)^2 + S_tK_S/(K_S + h)^2 \\ & + V_tK_V/(K_V + h)^2. \end{aligned} \tag{C33}$$

Note that for the simple case in which all the equilibria (27)–(29) lie far to the left, expression (C33) takes the form

$$D = 1 + [PGO]_tK_G/(K_G + h)^2 + F_tK_{F1}/(K_{F1} + h)^2. \tag{C34}$$

Substituting Eqs. (C3), (C6), (C7), (C9), (C11), and (C19) into Eq. (C32) gives

$$\begin{aligned} & 2v_S + v_3 - k_0(h + [OH^-]_0h/(K+h)) - k_0([F_eH] \\ & \quad + 2[F_eH_2] + [SH] + [VH]) - k_0'[PGOH] = (dh/dt)D. \end{aligned} \tag{C35}$$

Then Eqs. (C35), (C5)+(C6)+(C7), and (C2)+(C3), transform into the following equation:

$$\begin{aligned} dh/dt = {} & [2v_S + v_3 - k_0h - k_0[OH^-]_0h/(h+K) - k_0S_th/(h \\ & + K_S) - k_0F_th(2h + K_{F2})/(K_{F1}K_{F2} + hK_{F2} + h^2) \\ & - k_0V_th/(h + K_V) - k_0'[PGO]_th/(h + K_G)]/D, \end{aligned} \tag{C36}$$

$$dF_t/dt = 2v_S - k_0F_t, \tag{C37}$$

$$dS_t/dt = -2v_S - k_0(S_t - s_0), \tag{C38}$$

where

$$v_S = e_tS_tK_Sh(k_1K_e^2 + k_2h^2)/[(K_e^2 + h^2)(h + K_S)]. \tag{C39}$$

Equations (C8)+(C9) as well as (C10)+(C11) give $d[PGO]_t/dt = dV_t/dt = 0$. Since $v_3 \ll v_S$ for the reactant concentrations employed in our work, we can neglect v_3 in Eq. (C36) and omit Eq. (C17), since this last equation becomes uncoupled from the rest. After an initial transient, $F_t + S_t = s_0$, so Eq. (C37) can also be eliminated and F_t replaced by $(s_0 - S_t)$. Equations (C36) (with $v_3=0$) and (C38), together with Eqs. (C33) and (C39), can be taken as our "universal" equations for analysis of oscillations in GO-type systems. For simplicity, if the pH in the course of oscillations remains higher than 3.2, we can make the approximation that $K_S = K_{F2} = \infty$, i.e., neglect equilibria (27) and (28). Estimations and simulations also reveal that the term $k_0'([PGO]_t)h/(h + K_G)$ in (C36) is relatively small at our concentrations of e_t, $[OH^-]_0$, s_0, and $p\mathrm{H} < 5$, so it can be omitted. This simplifi-

cation is equivalent to the case of immobilized enzyme, when $k_0'=0$. Our equations then become

$$dh/dt = [2v_S - k_0 h - k_0[\mathrm{OH}^-]_0 h/(K+h) - k_0(s_0 - s)h/(K_{\mathrm{F1}}+h) - k_0 V_t h/(K_V+h)]/D, \tag{C40}$$

$$ds/dt = -2v_S - k_0(s - s_0), \tag{C41}$$

where v_S is given by Eq. (C18) and

$$D = [1 + N_{\mathrm{AG}} e_t K_{\mathrm{G}}/(K_{\mathrm{G}}+h)^2 + (s_0 - s)K_{\mathrm{F1}}/(K_{\mathrm{F1}}+h)^2 + V_t K_V/(K_V+h)^2]. \tag{C42}$$

APPENDIX D: SYMBOLS AND ABBREVIATIONS

$h=[\mathrm{H}^+]$, concentration of protons.

$s=[F_i]$, concentration of ferricyanide.

e_t, total concentration of all forms of enzyme glucose oxidase (GO).

v_e and v_S, rates of enzymatic reaction.

k_1 and k_2, rate constants of two-step autocatalytic reaction of GO with ferricyanide.

K_e, calculated constant in expression for v_S [Eqs. (30) and (34)] that determines the pH ($\cong pK_e$) at which autocatalysis switches from being characterized by constant k_1 to constant k_2.

K, parameter of computer-controlled negative feedback.

K_{G}, equilibrium constant for protonation of amino acid residues of GO.

N_{AG}, average number of protonatable residues of GO.

K_{F1} and K_{F2}, equilibrium constants for protonation of ferrocyanide, F_e, and $F_e\mathrm{H}$, respectively.

K_S, equilibrium constant for protonation of ferricyanide.

K_V, equilibrium constant for protonation of additional species V.

k_0, inverse residence time of the reactor.

APPENDIX E: DEPENDENCE OF k_2 ON $[\mathrm{Fe(CN)}_6^{3-}]_0$

From experimental curves like those shown in Fig. 3(a) we found that the slope in the slow stage of autocatalysis ["k_1" in Fig. 3(b)] is directly proportional to $[\mathrm{Fe(CN)}_6^{3-}]_0$, while the slope of the fast stage is proportional to $[\mathrm{Fe(CN)}_6^{3-}]_0^{1.5}$. Thus if one writes the rate equation in the usual form, in which the rate is directly proportional to the substrate concentration, k_2 [Eq. (30)] depends on $[\mathrm{Fe(CN)}_6^{3-}]_0^{0.5}$. One possible origin of the apparent dependence of k_2 on $[\mathrm{Fe(CN)}_6^{3-}]_0^{0.5}$ at relatively large concentrations of $[\mathrm{Fe(CN)}_6^{3-}]_0$ is that k_2 depends on the ionic strength.[51]

APPENDIX F: INHIBITION OF GO BY FERRICYANIDE AT LOW pH

We have found that if a solution of GO (ca. 1 mg/ml) is kept at pH 3 and room temperature for 10 min or more, its activity (the initial slope of the pH versus. time curve, as in Fig. 3) remains almost unchanged upon adding ferricyanide and glucose and setting the "initial" pH to 6. But if GO is kept with ferricyanide (ca. 10 mM) for 5 min under the same conditions, then the GO activity decreases almost to zero.

[1] B. Chance, A. Ghosh, and R. W. Estabrook, Proc. Natl. Acad. Sci. U.S.A. **51**, 1244 (1964).
[2] S. Dano, G. Sorensen, and F. Hynne, Nature (London) **402**, 320 (1999).
[3] B. Chance, A. Betz, and B. Hess, Biochem. Biophys. Res. Commun. **16**, 182 (1964).
[4] B. Hess and K. Brand, Biochem. Biophys. Res. Commun. **23**, 102 (1966).
[5] K. Eschrich, W. Schellenberger, and E. Hofmann, Arch. Biochem. Biophys. **222**, 657 (1983).
[6] H. F. Chou, N. Berman, and E. Ipp, Am. J. Physiol. **262**, E800 (1992).
[7] A. T. Harootunian, J. P. Y. Kao, S. Paranjape, and R. Y. Tsien, Science **251**, 75 (1991).
[8] J. Lechleiter, S. Girard, E. Peralta, and D. Clapham, Science **252**, 123 (1991).
[9] M. S. Nash, K. W. Young, R. A. J. Challiss, and S. R. Nahorski, Nature (London) **413**, 381 (2001).
[10] C. F. Hinks, Nature (London) **214**, 386 (1967).
[11] M. W. Mahowald and C. H. Schenck, Nature (London) **437**, 1279 (2005).
[12] A. L. Kindzelskii and H. R. Petty, Proc. Natl. Acad. Sci. U.S.A. **99**, 9207 (2002).
[13] H. R. Petty and A. L. Kindzelskii, Proc. Natl. Acad. Sci. U.S.A. **98**, 3145 (2001).
[14] S. Nakamura, K. Yokota, and I. Yamazaki, Nature (London) **222**, 794 (1969).
[15] A. Scheeline, D. L. Olson, E. P. Williksen, G. A. Horras, M. L. Klein, and R. Larter, Chem. Rev. (Washington, D.C.) **97**, 739 (1997).
[16] J. G. Lazar and J. Ross, Science **247**, 189 (1990).
[17] A. Boiteux, A. Goldbeter, and B. Hess, Proc. Natl. Acad. Sci. U.S.A. **72**, 3829 (1975).
[18] A. Ghosh and B. Chance, Biochem. Biophys. Res. Commun. **16**, 174 (1964).
[19] A. Goldbeter and S. R. Caplan, Annu. Rev. Biophys. Bioeng. **5**, 449 (1976).
[20] B. Hess, Q. Rev. Biophys. **30**, 121 (1997).
[21] B. D. Aguda and R. Larter, J. Am. Chem. Soc. **112**, 2167 (1990).
[22] P. O. Westermark and A. Lansner, Biophys. J. **85**, 126 (2003).
[23] P. Smolen, J. Theor. Biol. **174**, 137 (1995).
[24] C. G. Hocker, I. R. Epstein, K. Kustin, and K. Tornheim, Biophys. Chem. **51**, 21 (1994).
[25] T. Ohmori and R. Y. K. Yang, Biotechnol. Appl. Biochem. **20**, 67 (1994).
[26] T. Ohmori and R. Y. K. Yang, Biophys. Chem. **59**, 87 (1996).
[27] T. Ohmori, M. Nakaiwa, T. Yamaguchi, M. Kawamura, and R. Y. K. Yang, Biophys. Chem. **67**, 51 (1997).
[28] S. R. Caplan, A. Naparstek, and N. J. Zabusky, Nature (London) **245**, 364 (1973).
[29] A. Naparstek, D. Thomas, and S. R. Caplan, Biochim. Biophys. Acta **323**, 643 (1973).
[30] P. D. Shen and R. Larter, Biophys. J. **67**, 1414 (1994).
[31] V. K. Vanag, J. Phys. Chem. A **102**, 601 (1998).
[32] G. A. Frerichs and R. C. Thompson, J. Phys. Chem. A **102**, 8142 (1998).
[33] M. J. B. Hauser, A. Strich, R. Bakos, Z. Nagy-Ungvarai, and S. C. Müller, Faraday Discuss. **120**, 229 (2001).
[34] M. J. B. Hauser, N. Fricke, U. Storb, and S. C. Müller, Z. Phys. Chem. **216**, 375 (2002).
[35] V. Leskovac, S. Trivic, G. Wohlfahrt, J. Kandrac, and D. Pericin, Int. J. Biochem. Cell Biol. **37**, 731 (2005).
[36] M. K. Weibel and H. J. Bright, J. Biol. Chem. **246**, 2734 (1971).
[37] R. Wilson and A. P. F. Turner, Biosens. Bioelectron. **7**, 165 (1992).
[38] T. Takahashi and M. Mitsumoto, Nature (London) **199**, 765 (1963).
[39] G. Wohlfahrt, S. Trivic, J. Zeremski, D. Pericin, and V. Leskovac, Mol. Cell. Biochem. **260**, 69 (2004).
[40] K. Ogawa, T. Nakajima-Kambe, T. Nakahara, and E. Kokufuta, Biomacromolecules **3**, 625 (2002).
[41] I. R. Epstein and J. A. Pojman, *An Introduction to Nonlinear Chemical Dynamics* (Oxford University Press, New York, 1998).
[42] J. Boissonade and P. De Kepper, J. Phys. Chem. **84**, 501 (1980).
[43] V. K. Vanag and I. R. Epstein, Phys. Rev. E **71**, 066212 (2005).
[44] Y. Luo and I. R. Epstein, J. Am. Chem. Soc. **113**, 1518 (1991).
[45] V. K. Vanag, A. M. Zhabotinsky, and I. R. Epstein, J. Phys. Chem. A **104**, 11566 (2000).

[46] P. W. Atkins, *Physical Chemistry*, 6th ed. (Oxford University Press, New York, 1998), p. 175.
[47] If $d(p\mathrm{H})/dt=-k(k>0)$, we have $d(-\log_{10}[\mathrm{H}^+])/dt=-k$; then $2.303(1/[\mathrm{H}^+])d[\mathrm{H}^+]/dt=k$, and $d[\mathrm{H}^+]/dt=(k/2.303)[\mathrm{H}^+]$.
[48] G. Rábai and I. R. Epstein, Inorg. Chem. **28**, 732 (1989).
[49] G. Rábai and I. Hanazaki, J. Phys. Chem. **98**, 2592 (1994).
[50] J. Zagora, M. Voslar, L. Schreiberova, and I. Schreiber, Phys. Chem. Chem. Phys. **4**, 1284 (2002).
[51] J. Jordan and G. J. Ewing, Inorg. Chem. **1**, 587 (1962).
[52] G. Rábai, K. Kustin, and I. R. Epstein, J. Am. Chem. Soc. **111**, 3870 (1989).
[53] FLEXPDE, http://www.pdesolutions.com/ (2001).
[54] P. De Kepper, I. R. Epstein, and K. Kustin, J. Am. Chem. Soc. **103**, 2133 (1981).
[55] F. Sagués and I. R. Epstein, Dalton Trans. **7**, 1201 (2003).
[56] G. P. Misra and R. A. Siegel, J. Controlled Release **81**, 1 (2002).
[57] K. R. Dunbar and R. A. Heintz, Prog. Inorg. Chem. **45**, 283 (1997).
[58] J. Wagner and J. Keizer, Biophys. J. **67**, 447 (1994).
[59] C. J. Roussel and M. R. Roussel, Prog. Biophys. Mol. Biol. **86**, 113 (2004).